NEOPLASIA
www.neoplasia.com

Volume 10 Number 12 December 2008 pp. 1481–1492 1481

Variant HNF1 Modulates Epithelial Plasticity of Normal and Transformed Ovary Cells[1]

Antonella Tomassetti*, Giuseppina De Santis*, Giancarlo Castellano*, Silvia Miotti*, Mimma Mazzi*, Daniela Tomasoni*, Frans Van Roy†,‡, Maria Luisa Carcangiu§ and Silvana Canevari*

*Unit of Molecular Therapies, Department of Experimental Oncology, Fondazione IRCCS Istituto Nazionale dei Tumori, 20133 Milan, Italy; †Department of Molecular Biomedical Research, VIB, Ghent, Belgium; ‡Department of Molecular Biology, Ghent University, Ghent, Belgium; §Unit of Pathology C, Department of Pathology, Fondazione IRCCS Istituto Nazionale dei Tumori, 20133 Milan, Italy

Abstract

Ovarian carcinoma arises from the ovarian surface epithelium, which undergoes phenotypic changes characteristic of müllerian epithelium during the first stages of tumorigenesis. The variant isoform of the hepatocyte nuclear factor 1 (vHNF1) is a transcription factor involved in the development of tissues derived from the müllerian duct. Here, we show that vHNF1 knockdown in two ovarian carcinoma cell lines, SKOV3 and IGROV1, leads to reduced E-cadherin (E-cadh) expression and decreased proliferation rate. Accordingly, SKOV3 cells ectopically expressing a dominant-negative (DN) vHNF1 mutant undergo an epithelial-mesenchymal–like transition, acquiring a spindle-like morphology, loss of E-cadh, and disrupted cell-cell contacts. Gene expression profiling of DNvHNF1 cells on the basis of a newly compiled list of epithelial-mesenchymal transition–related genes revealed a correlation between vHNF1 loss-of-function and acquisition of the mesenchymal phenotype. Indeed, phenotypic changes were associated with increased Slug transcription and functionality. Accordingly, vHNF1-transfected immortalized ovarian surface epithelial cells showed down-regulation of Snail and Slug transcripts. In DNvHNF1-transfected SKOV3 cells, growth rate decreased, and in vHNF1-transfected immortalized ovarian surface epithelial cells, growth rate increased. By immunohistochemistry, we found a strong association of vHNF1 with E-cadh in clear cell and in a subset of serous carcinomas, data that could potentially contribute in distinguishing different types of ovarian tumors. Our results may help in understanding the biology of ovarian carcinoma, identifying early detection markers, and opening potential avenues for therapeutic intervention.

Neoplasia (2008) 10, 1481–1492

Introduction

The pathophysiology of epithelial ovarian cancers (EOCs) remains poorly defined. One widely supported hypothesis is that they are derived from inclusion cysts. These cysts originate from the ovarian surface epithelium (OSE), which is the monolayer of cells covering the ovaries [1,2]. Ovarian surface epithelium cells appear as a simple epithelium with some characteristics typical of mesenchymal cells. Ovarian surface epithelium cells remain plastic in short-term culture, expressing vimentin together with cytokeratins 8 and 18. Conversely, invaginations and inclusion cysts have properties characteristic of müllerian epithelium, including expression of the specific epithelial marker E-cadherin (cadh) at the cell-cell junctions. After transformation,

Abbreviations: Ab, antibody; cadh, cadherin; ctn, catenin; DN, dominant-negative; EMT, epithelial-mesenchymal transition; EOC, epithelial ovarian carcinoma; FR, folate receptor; IHC, immunohistochemistry; LMP, low malignant potential; MET, mesenchymal-epithelial transition; NE, nuclear extract; OSE, ovarian surface epithelium; vHNF1, variant hepatocyte nuclear factor; wt, wild type

Address all correspondence to: Antonella Tomassetti, Unit of Molecular Therapies, Department of Experimental Oncology, Fondazione IRCCS Istituto Nazionale dei Tumori, 20133 Milan, Italy. E-mail: antonella.tomassetti@istitutotumori.mi.it

[1]**Financial support:** This work was supported by grants to S.C. from Associazione Italiana Ricerca Cancro and the Cariplo Foundation, grant number 2003-1740.
Received 19 August 2008; Revised 13 October 2008; Accepted 13 October 2008

DOI 10.1593/neo.81004

EOC cells can coexpress E-cadh and the mesenchymal marker vimentin as well as epithelial cytokeratins [3]. Unlike the tumor suppressor function of E-cadh in breast, prostate, and colon carcinomas [4,5], expression of E-cadh in ovarian epithelium seems to be associated with the development of EOCs [6]. Nonetheless, the mechanism of E-cadh–associated malignant OSE transformation is controversial [7,8]. In some advanced-stage EOCs, the so-called mesenchymal-epithelial transition (MET), which occurs during the first stages of transformation, is followed by an epithelial-mesenchymal transition (EMT) with loss of E-cadh expression [9].

Epithelial-mesenchymal transition is required for morphogenesis during embryonic development but has also been implicated in the acquisition of invasiveness by end-stage tumors [10–12]. This conversion results in loss of expression of adhesion molecules, such as E-cadh, ZO-1, and occludin, with consequent loss of cell-cell contacts and extensive remodeling of the cytoskeleton. Loss of E-cadh during development and cancer progression in tumors, other than EOCs, is mainly caused by transcriptional repression resulting from interaction of regulators with specific E-boxes in the proximal promoter of *Cdh1*, the gene encoding E-cadh [13]. Most prominent in this respect are the Snail-related zinc-finger transcription factors Snail and Slug.

The variant isoform of the transcription factor HNF-1 (vHNF1) activates transcription on homodimerization or heterodimerization with its companion protein HNF1α [14]. A role for HNF1 proteins in tumors has not yet been defined. For HNF1α, a biallelic inactivation of the relevant gene has been found in 50% of human liver adenomas [15], and somatic mutations were observed in 11% of endometrial carcinomas but not in breast and ovarian carcinomas [16]. Regarding vHNF1, the complete inactivation by germ line mutation of *TCF2*, the gene encoding for vHNF1, seemed to be associated to renal cell carcinoma [17] hypothesizing a tumor suppressor function. More recently, two variants within TCF2 have been found to be associated to prostate cancer risk [18]. vHNF1 is involved in the development of tissues organized in tubules, such as the pancreatic exocrine ducts and the kidney tubules [19,20], and in müllerian duct–derived tissues [21]. The transcription of the *FR* gene, which encodes the folate receptor (FR) α, is strongly activated in EOCs. We recently showed that the *FR* gene is regulated by vHNF1 [22], which is expressed in ovarian tumor specimens but not in OSE cells or in specimens obtained from tumors of other oncotypes.

Here, we addressed the potential role of vHNF1 in the MET-like taking place during ovarian cell transformation. We used *in vitro* approaches to negatively or positively affect vHNF1 expression and/or functionality in ovarian normal and transformed cells. We found that vHNF1 expression and functionality are directly correlated with epithelial differentiation, positively associated with growth potential, and inversely correlated with expression and functionality of E-box–binding transcriptional repressors. Immunohistochemical analysis of normal and transformed ovarian tissues showed that vHNF1 is not expressed in OSE cells but is expressed in 33% of E-cadh–expressing EOCs independently of tumor grading. The overall results demonstrate that vHNF1 is a new player in the epithelial differentiation of a subset of normal and transformed ovary cells.

Materials and Methods

Cell Culture

The ovarian carcinoma cell lines IGROV1 and SKOV3 (American Type Culture Collection, Manassas,VA) were maintained in RPMI 1640 medium (Sigma, St. Louis, MO) supplemented with 10% FCS (Sigma) and 2 mM L-glutamine. hTERT-IOSE (hereafter designated IOSE), obtained as described [23], were maintained in 199-MCDB105 medium (Sigma) supplemented with 15% FCS, 2 mmol L-glutamine, 200 μg/ml G418, and 50 μg/ml hygromycin.

Reagents and Antibodies

Triton X-100 (TX-100) and MES were from Sigma-Aldrich Fine Chemicals (St. Louis, MO); geneticin sulfate (G418) was from Gibco BRL (Paisley, Scotland). The following primary antibodies (Abs) were used at the dilution recommended by the manufacturer: anti-vHNF1 (goat), anti-HNF1 (rabbit), anti–ZO-1, and anti–occludin 1 (Santa Cruz Biotechnology, Santa Cruz, CA); anti–E-cadh mAb (mouse; Transduction Laboratories, BD Biosciences Pharmingen, Palo Alto, CA); anti-S100A4 (rabbit; DakoCytomation, Glostrup, Denmark). Horseradish peroxidase–labeled secondary Abs were from Amersham Bioscience–GE Healthcare (Piscataway, NJ). Secondary fluorochrome–conjugated Alexa Fluor 488 (green) was from Molecular Probes (Eugene, OR).

Small interfering RNA Treatment

IGROV1 and SKOV3 cells (5×10^5) were seeded in 24-well plates and transfected 24 hours later with 80 pmol/ml of small interfering RNA (siRNA) duplex against vHNF1 mRNA (SmartPool; Dharmacon, Lafayette, CO) or Luciferase siRNA as control (Quiagen-Xeragon, Germantown, MD). siRNA transfection was performed by using Lipofectamine 2000 (Invitrogen, Paisley, UK) according to the manufacturer's protocol. Cells were harvested 48 hours later and analyzed for RNA and protein expression by quantitative reverse transcription–polymerase chain reaction (RT-PCR) and Western blot analysis, respectively.

Construction of DNvHNF1 and vHNF1 Expression Vectors

vHNF1 cDNA was obtained from the vector RSV-LFB3 (kindly provided by C. Toniatti, IRBM, Merck Research Laboratories, Pomezia, Italy). Dominant-negative vHNF1 (DNvHNF1; nt 1-729 of the open reading frame) was obtained by standard PCR with sense and antisense primers containing *Hin*dIII and *Xba*I restriction sites, respectively (sense, 5′-AGGAGGTCTAGAATGGTGTCCAAGCTCACG-3′; antisense, 5′-AAGGGAAGCTTTCACCAGGCTTGTAGAGG-3′). The purified fragment was inserted into the *Hin*dIII and *Xba*I sites of the expression vector pcDNAIneo (Invitrogen). For the expression vector encoding vHNF1, the vHNF1 open reading frame was inserted into the *Hin*dIII and *Xba*I restriction sites of the pcDNA3.1/Hygro vector (Invitrogen). Before transfection, both vHNF1-pcDNA3.1/Hygro and DNvHNF1-pcDNAIneo were verified by sequencing.

Quantitative Real-time RT-PCR

Total RNA was isolated with the RNeasy Total RNA kit (Quiagen, Hilden, Germany) according to the manufacturer's instructions. One microgram of total RNA was reverse-transcribed using the ABI High Capacity cDNA Archiving Kit (Applied Biosystem, Foster City, CA). Three replicates were run for each gene in each sample in a 96-well format plate. The probes and primer sets were the following Assays on Demand: Ref Hs00170423_m1 for *Cdh1*, Hs00195591_m1 for *Snail*, Hs00161904_m1 for *Slug*, HS00170182_mi for *PLAU*, and Hs00277509_m1 for *FN* (Applied Biosystems). *GADPH* mRNA levels were used as a control for the RNA extraction and RT experiments. Data were analyzed with the Sequence Detector v1.9 software. Relative

gene expression for each sample was determined using the formula $2^{(-\Delta Ct)}$ reflecting target gene expression normalized to *GAPDH* levels.

Cell Solubilization, Fractionation, and Western Blot Analysis

For preparation of total cell lysates, cells were washed with ice-cold PBS and lysed in SDS sample buffer (62.5 mM Tris-HCl pH 6.8, 2.3% SDS, 10% glycerol, 5% β-mercaptoethanol, 0.005% bromophenol blue). Proteins were separated on precast 4% to 12% SDS-PAGE (Invitrogen) and transferred onto nitrocellulose membranes (Amersham Bioscience–GE Healthcare) as described [24]. Visualization was by the enhanced chemiluminescence method (Amersham Biosciences) using a Chemidocxrs and the Quantity One software (Bio-Rad, Hercules, CA). For cellular fractionation, confluent cells were treated as described [24]. Protein concentration of the fractions was determined by the BCA protein reagent assay (Pierce, Rockford, IL).

Cell Transfection

IGROV1 and SKOV3 cells were transfected with the DNvHNF1 construct essentially as described [25] using Lipofectamine 2000 according to the manufacturer's suggestions (Invitrogen). Forty-eight hours after transfection, fresh medium containing 400 μg/ml G418 (Gibco BRL) was added to the cell culture. DNvHNF1-positive clones were identified by RT-PCR using oligonucleotides that amplify only DNvHNF1 but not wild type (wt) vHNF1 (data not shown). Stable clones were tested by Western blot analysis on total cell lysates using rabbit anti-HNF1 Ab, which recognized both wt and DNvHNF1 proteins (Santa Cruz Biotechnology).

Immunofluorescence

Immunofluorescence was performed essentially as described [24], 2×10^4 cells seeded on glass coverslips were grown for 48 hours, washed with cold PBS, and fixed with cold methanol for 10 minutes before immunoreaction. Samples were mounted with Mowiol solution and examined with an Eclipse TE2000-S microscope with a 40× PanFluor objective (Nikon, Melville, NY). Images were acquired with ACT-1 software (Nikon) at a resolution of 2250 × 1800 pixels. All procedures were carried out at room temperature.

Electrophoretic Mobility Shift Assay

Preparation of nuclear extracts (NEs) and electrophoretic mobility shift assay were carried out essentially as described [22].

Microarray Analysis

Gene expression in DNvHNF1 and mock transfectants was compared in three different RNA preparations pooled for each cell line. Total RNA from transfected SKOV3 cultures was extracted, further purified on RNeasy Mini Kit (Qiagen, Valencia, CA) according to the manufacturer's protocols, and treated with DNase (RNase-free DNase Set; Qiagen). Targets were obtained by synthesizing cDNA from 15 μg of total RNA. To verify the reproducibility of the observations, we performed two separate retrotranscriptions from both cell types to obtain four separate targets for hybridization. Genome set Human U133 Plus 2.0 chips (Affymetrix, Santa Clara, CA) were used in duplicate. Data from the two biologic replicates for each target (DNvHNF1 and mock cells) were tested in duplicate chips (a total of four samples for target) after normalization. The statistical analyses of the microarray data were performed with GenePicker software designed by the IFOM Institute (Milan, Italy). This software allowed to set up analysis schemes and to search the data for regulated genes using *t* test and Change-Fold Change analysis. We performed the reported analysis selecting the probe sets with significant statistical analysis ($P < .05$ for *t* test) and a fold change >1.5 or <–1.5, obtaining a list of 621 probe sets.

Compilation of Gene Lists Associated with the Epithelial or Mesenchymal Phenotype

A list of EMT-related genes was compiled after a literature search for genes modulated during processes activated by EMT [10,12] and taking into consideration two studies of gene expression profiling: one on Ha-*ras*–transformed polarized mammary epithelial cell line EpH4 induced to EMT by TGFβ treatment [26] and another on Madison-Darby canine kidney epithelial cells expressing the E-box–binding repressors Snail, Slug, and E47 [27]. Table W1 shows a list of genes associated with epithelial (140) and mesenchymal (186) phenotypes and passing criteria as that reported above. The categorization reported in both Tables 1 and W1 was done according to the Gene Ontology categories.

Luciferase *Assay*

Cells were transfected with TOP- and FOP-promoter–reporter gene constructs (Upstate Biotechnology, Lake Placid, NY) using Lipofectamine 2000 according to the manufacturer's suggestions (Invitrogen). Cotransfection with thymidine kinase–Renilla was performed to evaluate transfection efficiency. After 48 hours, cells were lysed and analyzed for promoter activity. The dual-luciferase assay was performed essentially as suggested by the manufacturer (Promega, Madison, WI).

Growth Potential Measurements

In vitro proliferation of stable transfected cells was measured with the CellTiter-Glo luminescent cell viability assay kit (Promega) according to the manufacturer's suggestions. Cells (4×10^4 cells per well) were cultured in 96-well plates for up to 5 days. *In vitro* proliferation of siRNA-treated cells was evaluated as radiolabeled thymidine incorporation. Briefly, cells were plated in 96-well plates at a density of 1×10^4 cells per well and transiently transfected with siRNA duplex against vHNF1 mRNA or control siRNA. Cells were pulsed for 4 hours with [*methyl*-^{3}H]thymidine (Amersham; 1 μCi per well) and 24 (for IGROV1 cells) or 48 hours (for SKOV3cells) later washed twice with ice-cold PBS. After fixation with 100 μl of 10% trichloroacetic acid for 30 minutes at 4°C, cells were lysed with 100 μl per well 0.2 N NaOH and radiolabeled thymidine incorporation was measured by scintillation counting.

Immunohistochemistry

All clinical specimens were obtained with approval from the institutional review board and informed consent from all participating patients to use excess biologic material for investigative purposes. Immunohistochemistry (IHC) was performed by using routine tissue blocks and a commercially available tissue arrays (Ovary cancer, AccuMax Array, Petagen and CJ1 Human, Ovary cancer, and Super Bio Chips) essentially as described [28]. For antigen retrieval and primary Ab dilutions, see Supplementary data. Two observers (M.L.C. and A.T.) independently assessed positivity or negativity of staining on the basis of intensity and the percentage of positive cells.

Statistical Analyses

GraphPad Prism software (GraphPad Software, San Diego, CA) was used to analyze all data. Differences between mean values were determined by Student's *t* test, and Fisher's test was used to determine

Table 1. Genes Associated with Epithelial and Mesenchymal Phenotypes* and Found to Be Differentially Expressed in DNvHNF1 *Versus* Mock Cells.

Gene Symbol	GenBank ID	Gene Name	Fold Change	*P*
Epithelial genes (n = 134)†				
Actin cytoskeleton organization (*n* = 6)				
PODXL	NM_005397	podocalyxin-like	1.94	.0002
Cell adhesion/ECM–related (*n* = 22)				
ANXA4	BC000182	annexin A4	−1.84	.0000
CD99	U82164	CD99 antigen	1.66	.0000
CDH1	NM_004360	cadherin 1, type 1, E-cadherin	−3.33	.0404
CLDN1	AF101051	claudin 1	−2.07	.0002
CLDN7	NM_020412	claudin 7	−7.26	.0000
EVA1	AF275945	epithelial V-like antigen 1	3.00	.0002
FBLP-1	AL133035	filamin-binding LIM protein-1	−3.01	.0131
ITGA3	NM_002204	integrin, alpha 3	1.62	.0002
ITGB6	AK026736	integrin, beta 6	2.50	.0002
PDZK1IP1	NM_005764	PDZK1-interacting protein 1	−2.03	.0000
NID2	NM_007361	nidogen 2	−1.91	.0005
OCLN	AI829721	occludin	−1.70	.0512
Cell cycle (*n* = 8)				
DUSP1	NM_004417	dual-specificity phosphatase 1	−1.94	.0053
Cell growth/maintenance (*n* = 42)				
BPAG1	AI798790	bullous pemphigoid antigen 1, 230/240 kDa	1.64	.0000
DEFB1	U73945	defensin, beta 1	−7.78	.0000
GDI2	D13988	GDP dissociation inhibitor 2	−1.86	.0000
SEMA3C	NM_006379	sema domain, immunoglobulin domain (Ig), secreted, (semaphorin) 3C	6.22	.0000
TACSTD2	J04152	tumor-associated calcium signal transducer 2	−4.03	.0325
Cell motility (*n* = 8)				
F11R	AF154005	F11 receptor	−2.09	.0325
JAG1	U77914	jagged 1	2.19	.0000
Metabolism (*n* = 29)				
CA2	M36532	carbonic anhydrase II	−17.04	.0000
CITED2	AF109161	Cbp/p300–interacting factor, with Glu/Asp–rich carboxy-terminal domain, 2	−2.02	.0340
EXT1	NM_000127	exostoses (multiple) 1	−1.63	.0005
Mesenchymal genes (n = 173)				
Actin cytoskeleton organization (*n* = 9)				
ACTN1	AI082078	actinin, alpha 1	1.9	.0005
PLEK2	NM_016445	pleckstrin 2	2.02	.0008
Cell adhesion/ECM–related (*n* = 21)				
BGN	BC002416	biglycan	10.5	.0000
CD44	AF098641	CD44 antigen	2.10	.0000
COL5A1	NM_000393	collagen, type V, alpha 1	2.05	.0000
COL5A2	AL564683	collagen, type V, alpha 2	39.29	.0000
FN1	AK026737	fibronectin 1	−10.39	.0425
Lamb1	M20206	laminin, beta 1	2.91	.0000
Cell cycle (*n* = 10)				
CDC2	NM_001786	cell division cycle 2, G_1 to S and G_2 to M	−1.69	.0523
Cell growth and/or maintenance (*n* = 59)				
CXCL1	NM_001511	chemokine (C-X-C motif) ligand 1	−1.78	.0015
EPS8	NM_004447	epidermal growth factor receptor pathway substrate 8	2.07	.0000
FZD1	NM_003505	frizzled homolog 1	1.86	.0006
FZD2	L37882	frizzled homolog 2	1.66	.0001
HMGA2	NM_003483	high mobility group AT-hook 2	2.76	.0001
IGFBP1	NM_000596	insulin-like growth factor binding protein 1	−9.94	.0067
IGFBP3	M31159	insulin-like growth factor binding protein 3	−2.90	.0006
KIFAP3	NM_014970	kinesin-associated protein 3	2.71	.0067
Met	BG170541	met proto-oncogene (hepatocyte growth factor receptor)	2.77	.0015
PMP22	L03203	peripheral myelin protein 22	2.05	.0013
PTPRM	NM_002845	protein tyrosine phosphatase, receptor type, M	−2.74	.0013
SLC29A1	AF079117	solute carrier family 29 (nucleoside transporters), member 1	1.90	.0003
Cell motility (*n*= 25)				
MMP10	NM_002425	matrix metalloproteinase 10 (stromelysin 2)	3.59	.0000
MMP2	NM_004530	matrix metalloproteinase 2	4.10	.0000
MMP7	NM_002423	matrix metalloproteinase 7	7.51	.0000
PLAU	NM_002658	plasminogen activator, urokinase	2.90	.0000
PLAUR	X74039	plasminogen activator, urokinase receptor	4.02	.0000
S100A2	NM_005978	S100 calcium binding protein A2	2.20	.0000
S100A3	NM_002960	S100 calcium binding protein A3	2.04	.0004
S100A4	NM_002961	S100 calcium binding protein A4	2.05	.0000
S100A6	NM_014624	S100 calcium binding protein A6	1.64	.0001
S100P	NM_005980	S100 calcium binding protein P	−29.48	.0002
SERPINH1	BF316352	serine (or cysteine) proteinase inhibitor	−2.44	.0000
Development/differentiation (*n* = 23)				
ID1	D13889	inhibitor of DNA binding 1, dominant negative helix-loop-helix protein	−1.94	.0000
ID3	NM_002167	inhibitor of DNA binding 3, dominant negative helix-loop-helix protein	−23.23	.0001

Table 1. (*continued*)

Gene Symbol	GenBank ID	Gene Name	Fold Change	*P*
ID4	U16153	inhibitor of DNA binding 4, dominant negative helix-loop-helix protein	−3.89	.0001
LUM	NM_002345	lumican	18.65	.0001
SNAI2	AI572079	snail homolog 2 (*Drosophila*)	4.91	.0000
SPARC	NM_003118	secreted protein, acidic, cysteine-rich (osteonectin)	8.94	.0000
Metabolism (*n* = 22)				
ACVR1	NM_001105	activin A receptor, type I	2.74	.0045
BHLHB2	NM_003670	basic helix-loop-helix domain containing, class B, 2	2.36	.0000
PTGIS	NM_000961	prostaglandin I2 (prostacyclin) synthase	−2.17	.0012
Biological process unknown (*n* = 3)				
PSTPIP2	NM_024430	proline-serine-threonine phosphatase interacting protein 2	−2.67	.0003
UPP1	NM_003364	uridine phosphorylase 1	−2.80	.0000

*The genes listed in the EMT-related gene database (Table W1) were extracted from the DNvHNF1/Mock data set generated using the GeneChip Human Genome U133 Plus 2.0 Array. Note that 307 (94%) of 326 EMT-related genes were present in the chip.
†The total number of genes belonging to each category is shown in parentheses.

whether the percentage of EMT-related genes is different by chance. The correlation of vHNF1 and E-cadh expression levels in IHC was evaluated by χ^2 test. *P* values <.05 (2-sided) were considered significant.

Results

vHNF1 Silencing Impairs Epithelial Differentiation of Ovarian Tumor Cells

To identify the role of vHNF1 in ovarian carcinoma cells, IGROV1 and SKOV3 cells were transfected with vHNF1-specific siRNA or control siRNA (Figure 1*A*). The reduction of endogenous vHNF1 transcription and protein expression correlated directly with a decrease in the levels of E-cadh transcription and protein expression in both cell lines. The decreased intensity of the 120-kDa band corresponding to the full-size E-cadh protein in lysates of vHNF1 siRNA-treated cells (Figure 1*B*) was not caused by degradation [29] because proteins of lower molecular weight were equally abundant in all lysates.

Further, we measured the growth capability of IGROV1 and SKOV3 cells treated with vHNF1-specific siRNA (Figure 1*C*). By radiolabeled thymidine incorporation, we observed that reduction of endogenous vHNF1 expression led to a 25% (*P* = .026) and 45% (*P* = .018) decrease in proliferation of IGROV1 and SKOV3 cells, respectively.

vHNF1 Loss-of-Function Impairs Epithelial Differentiation of Ovarian Tumor Cells

o scrutinize the role of vHNF1 expression in ovarian carcinomas, we stably transfected IGROV1 and SKOV3 cells with an expression plasmid containing a DNvHNF1 cDNA encoding the truncated vHNF1 form that occurs naturally in pancreatic β-cells of patients bearing maturity-onset diabetes of the young type 5 (Figure 2*A*) [30]. We were unable to obtain any stable clone despite repeated DNvHNF1 transfections in IGROV1 cells (data not shown), but we obtained several stable clones by transfecting SKOV3 cells. Western blot analysis of total cell lysates from DNvHNF1-transfected SKOV3 clones (hereafter designated DNvHNF1) using an Ab that detects both wt vHNF1 and DNvHNF1 revealed the truncated 27-kDa band only in DNvHNF1 cells (Figure 2*B*). Probing the same blots with an Ab against E-cadh showed a large decrease in the expression of this protein in all DNvHNF1 clones analyzed. Furthermore, we obtained the same results on transfection of MDCK cells with the same construct (data not shown). Clone 1 was further characterized.

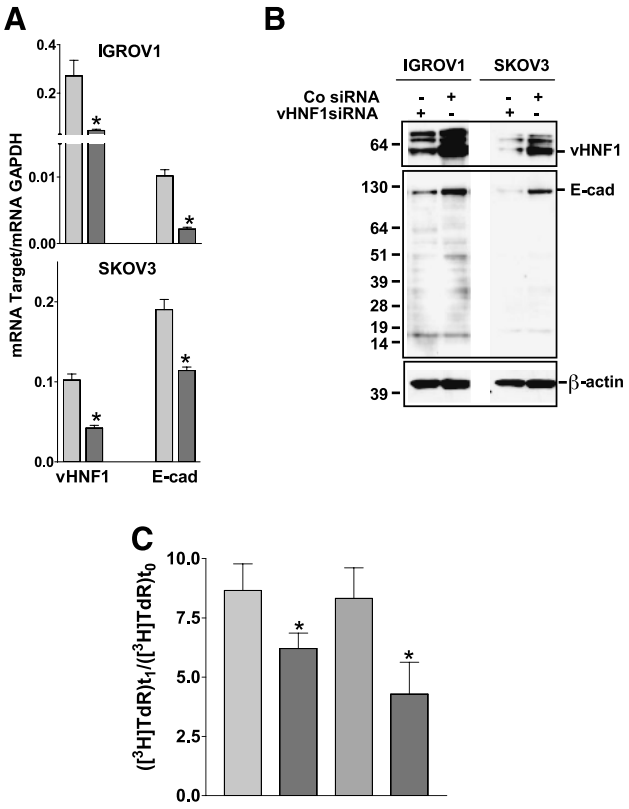

Figure 1. vHNF1 silencing impairs epithelial differentiation of ovarian tumor cells. IGROV1 and SKOV3 cells were treated with a vHNF1-specific siRNA. (A) Quantitative RT-PCR on total RNA extracts from cells treated with a control (light gray bar) or vHNF1-specific (dark gray bar) siRNA. Data represent mean (SD) for the vHNF1 and E-cadh genes normalized to the housekeeping gene *GAPDH* in at least six determinations. Asterisks indicate significant differences ($P < .05$). (B) In a parallel experiment, cells were lysed and analyzed by Western blot analysis with Abs against vHNF1 and E-cadh, respectively. *Co siRNA* indicates control siRNA. β-Actin was used for normalization of gel loading. One of three experiments is shown. (C) IGROV1 and SKOV3 cells were treated with a control (light gray bar) or a vHNF1-specific (dark gray bar) siRNA as in Figure 2, and proliferation was evaluated by incorporation of radiolabeled thymidine. Data are mean (SD) of six replicates; one of two experiments is shown. Asterisks indicate significant differences ($P < .05$).

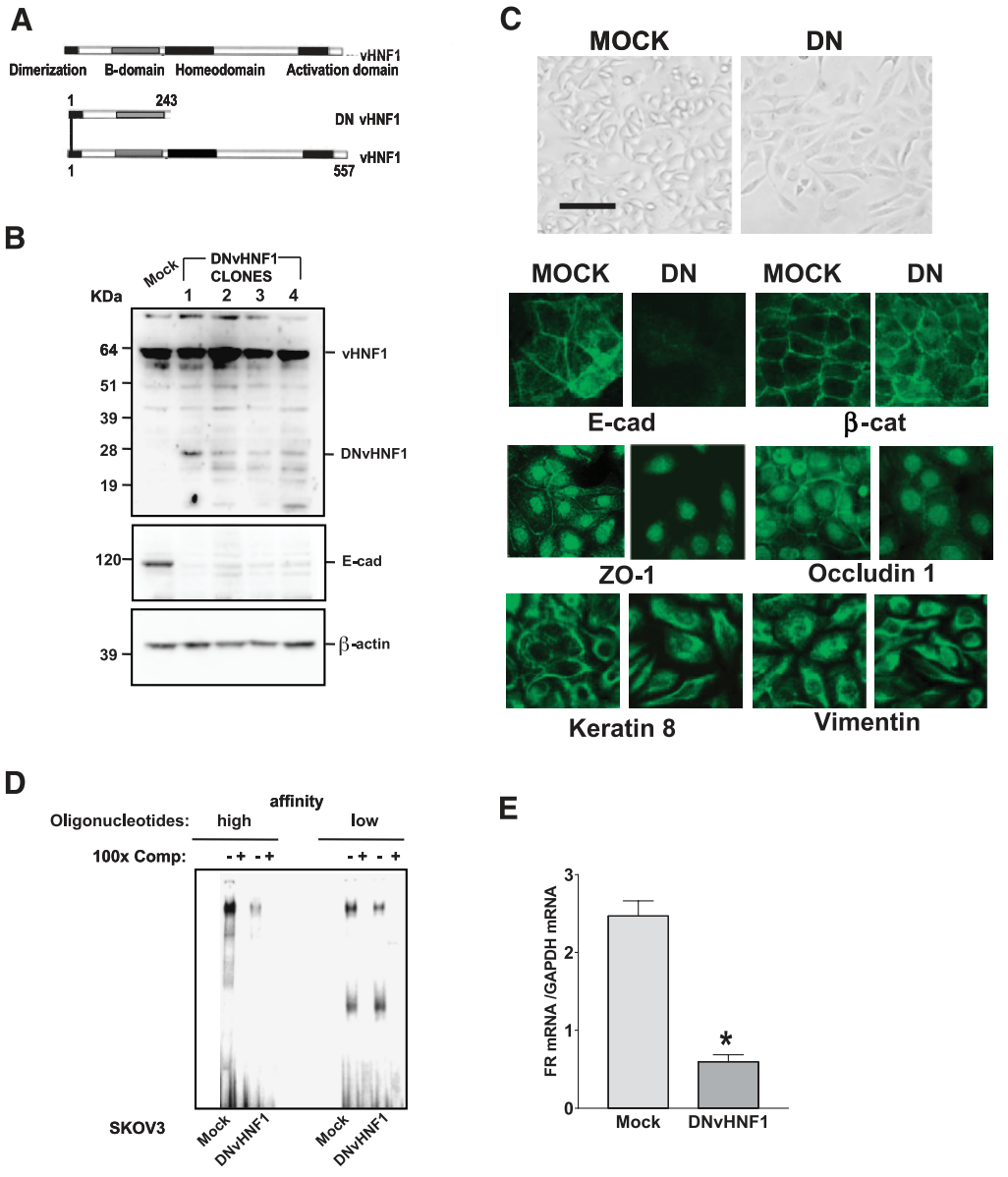

Figure 2. vHNF1 loss-of-function impairs epithelial differentiation of ovarian tumor cells. (A) Schematic representation of wt vHNF1, with its functional domains, and the truncated DNvHNF1. Note that DNvHNF1 only maintains the N-terminal dimerization and B domains. (B) Western blot analysis of total cell lysates from Mock cells and DNvHNF1 clones was performed using a rabbit anti-HNF1 Ab. The 15- to 24-kDa bands in DNvHNF1 lysates might represent shorter DNvHNF1 products; β-actin was used for normalization of gel loading. (C) Upper panel: Morphology of Mock and DNvHNF1 cells. Cells were grown to confluence in six-well plates, and images were obtained by phase-contrast microscopy with a 10× objective. Bar, 100 μm. Lower panel: IF was performed on methanol-fixed Mock and DNvHNF1 cells with Abs against the molecules indicated. Images were obtained with a 40× objective. (D) Electrophoretic mobility shift assay of NEs prepared from Mock and DNvHNF1 cells was performed using two oligonucleotides containing the HNF1 consensus DNA-binding site and corresponding to the proximal elements of the sequences of the *albumin* (high affinity) and *FR* (low affinity) promoters, respectively. Specific DNA-protein complexes were competed with a 100-fold molar excess of unlabeled probes (100× Comp), as indicated. (E) Quantitative RT-PCR of the FR transcript using total RNA extracted from Mock and DNvHNF1 transfectants. Data represent mean (SD) for FR expression normalized to the housekeeping gene *GAPDH* in at least six determinations. Asterisk indicates a significant difference ($P < .01$).

Consistent with the loss of E-cadh expression, in phase-contrast microscopy DNvHNF1 clones revealed a spindle-like shape and loss of defined cell-cell borders compared with the more epithelial morphology of mock-transfected cells (hereafter referred to as Mock cells; Figure 2*C*, *upper panel*). Immunofluorescence analysis of adherens junctions showed that E-cadh and β-catenin (ctn) expressions were confined to cell-cell contacts in Mock cells, whereas in DNvHNF1 cells, there was loss of E-cadh staining and discontinuous β-ctn staining at cell-cell contacts (Figure 2*C*, *lower panel*). Moreover, both ZO-1 and occluding 1, markers of tight junctions, were clearly present at cell-cell contacts in Mock cells, but they were mainly concentrated in the nuclei of DNvHNF1 cells, as previously shown in other cell systems [31,32]. Normal and transformed ovarian cells may display both epithelial and mesenchymal features [3], and accordingly,

SKOV3 cells coexpress both cytokeratins and vimentin. Interestingly, DNvHNF1 cells maintained coexpression of cytokeratins and vimentin but failed to display the typical pattern of cell-cell junctional cytokeratin filaments observed in Mock cells. Similar expression patterns were seen in the other DNvHNF1 clones (data not shown).

Electrophoretic mobility shift assay was performed with NEs from DNvHNF1 cells using two different vHNF1-specific oligonucleotides corresponding to the proximal elements of the sequences of the albumin (high affinity) and FR (low affinity) promoters [22,33]. This analysis indicated that the ability of NEs from DNvHNF1 cells to form DNA complexes with the oligonucleotides was substantially reduced compared to those from Mock cells (Figure 2*D*). On the basis of our previous demonstration that vHNF1 binds to and activates the *FR* promoter in ovarian carcinoma cells, we evaluated the FR transcript levels in DNvHNF1 cells to confirm the effective down-regulation of endogenous vHNF1 transcriptional activity by expression of the DNvHNF1 protein. Indeed, real-time RT-PCR analysis revealed a fourfold lower level of the FR transcript in DNvHNF1 cells (Figure 2*E*).

vHNF1 Loss-of-Function Induces a Gene Expression Profile Resembling That of EMT

We compared the gene expression profiles of DNvHNF1 cells and Mock cells by the GeneChip Human Genome U133 Plus 2.0 Array. Using a cutoff of 1.5-fold, we identified 459 upregulated and 473 downregulated genes in DNvHNF1 cells. A preliminary analysis of the differentially expressed genes indicated a pattern suggestive of EMT (data not shown). Thus, we focused on EMT and compiled a list of specific epithelial (140) and mesenchymal (186) genes that are reported in Table W1 (for list compilation, refer to the Materials and Methods section). In the epithelial gene list, genes associated with cell growth/maintenance, metabolism, cell adhesion/extracellular cell matrix (ECM)–related, and development/differentiation were the largest classes; in the mesenchymal gene list, cell growth/maintenance and cell motility–associated genes formed the largest classes. We extracted the expression data for each gene of this EMT-related list from the DNvHNF1 *versus* Mock data sets. A search for variation of expression of these genes in DNvHNF1 cells was consistent with our initial observation: 22% (67/307) of EMT-related genes were expressed differently in the two cell lines (Table 1), compared to the 13% expected by chance ($P < .0001$). More specifically, 24 of 134 epithelial genes in DNvHNF1 cells were differentially expressed: 16 of them were down-regulated and 8 were upregulated, which is consistent with published EMT data [26,27] (Figure 3*A*). In addition, 43 of 173 mesenchymal genes were differentially expressed and 29 of them (67%) were up-regulated in DNvHNF1 cells. Most modulated genes in DNvHNF1 cells were associated with cell adhesion/ECM (18 genes), cell growth/maintenance (16 genes), or motility (13 genes). Among the mesenchymal genes, we observed up-regulation of *CD44*, *Met*, *PLAU*, *PLAUR*, *MMP2*, *MMP7*, *S100A4*, *HMG2A*, *SNAI2*, and *SPARC*, all of which are expressed during EMT. Real-time RT-PCR for *PLAU* showed up-regulation of these genes in DNvHNF1 cells (Figure 3*B*). Western blot analysis with anti-S100A4 Ab indicated increased expression of this protein in DNvHNF1 cells compared to Mock cells (Figure 3*C*). Among epithelial genes, we found down-regulation of *CDH1*, which encodes E-cadh, and *OCLN*, which encodes for occluding, that had been shown before to be downregulated in DNvHNF1 cells (Figure 2), and *TACSTD2*, encoding Ep-CAM protein, which is highly expressed in ovarian carcinoma cells [34].

Some apparent discrepancies with published data were found, such as the up-modulation of *ITGB6* and *SEMA3C*, described before as down-modulated in the epithelial phenotype [26], and the down-regulation of typical mesenchymal genes, such as *FN* and *IDs* [9,35]. Nevertheless, real-time RT-PCR confirmed the down-regulation of *FN* in DNvHNF1 cells (Figure 3*B*).

These results strongly suggest that vHNF1 loss-of-function impairs cell-cell adhesion and leads to a more mesenchymal phenotype in the SKOV3 ovarian carcinoma cell line.

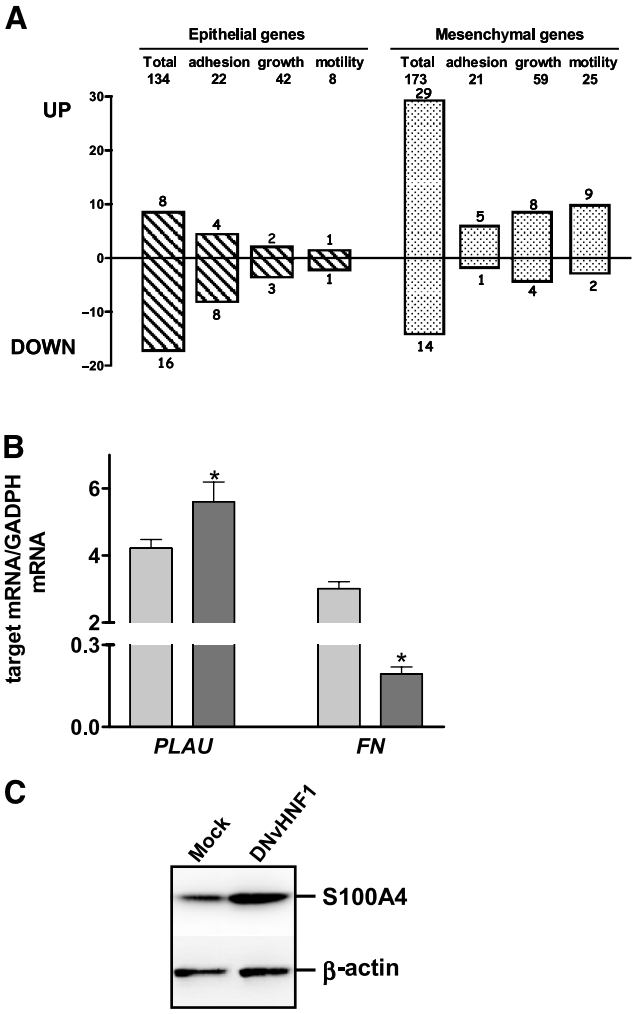

Figure 3. vHNF1 loss-of-function induces a gene expression profile resembling that of EMT. (A) Upper panel: we compiled a list of specific epithelial (134) and mesenchymal (173) genes that are reported in Table W1. The number of genes in the largest functional classes is reported. Lower panel: we extracted the expression data for each gene of this EMT-related list from the DNvHNF1 *versus* Mock data sets. Epithelial (dashed bars) and mesenchymal (dotted bars) genes differentially expressed in DNvHNF1 *versus* Mock data sets. (B) Quantitative RT-PCR for target mRNA was performed with total RNA extracted from Mock (light gray bars) and DNvHNF1 (dark gray bars) cells. Data represent mean (SD) for the relevant genes normalized to the housekeeping gene *GAPDH* in at least six determinations. Asterisks indicate significant difference ($P < .02$). (C) Western blot analysis of total cell lysates from Mock and DNvHNF1 cells was performed using a rabbit anti-S100A4 Ab. β-Actin was used for normalization of gel loading. One of three gels is shown.

vHNF1 Loss-of-Function Leads to Slug Expression and Functionality

E-cadh down-regulation could have been caused by transcriptional repression by E-box transcription factors, so we performed quantitative real-time RT-PCR to evaluate the expression of E-cadh and its transcriptional regulators Snail and Slug. Compared to Mock cells, DNvHNF1 cells showed absence of E-cadh mRNA, 2-fold decreased Snail mRNA levels, and 1.8-fold increased Slug mRNA levels (Figure 4*A*). We then analyzed in these cell lines the effect of vHNF1 loss-of-function on *Cdh1* promoter activity (Figure 4*C*) by transiently transfecting the promoter constructs depicted in Figure 4*B*. Luciferase reporter assay showed that the activity of the E-box–containing *Cdh1* promoter significantly decreased about threefold in DNvHNF1 cells compared to Mock cells. The activities of the mutated E-box–containing construct were less derepressed in DNvHNF1 cells than in Mock cells, indicating that in DNvHNF1 cells, other mechanisms may contribute to the repression of the *Cdh1* promoter in addition to the activity of E-box–binding proteins.

These results indicate that loss of E-cadh expression in DNvHNF1 cells might be caused by transcriptional repression partly mediated by Slug binding to specific E-boxes of the *Cdh1* promoter.

Ectopic Expression of vHNF1 in IOSE Cells Is Sufficient to Induce Snail and Slug

The data presented above indicate that vHNF1 participates in determining the epithelial phenotype of ovarian cancer cells. To evaluate whether vHNF1 is sufficient to activate a differentiation program toward MET in normal ovary cells, we stably transfected hTERT-IOSE cells [23] with vHNF1 cDNA. Western blot analysis with anti-vHNF1 Ab revealed that two selected clones of vHNF1-transfected hTERT-IOSE (hereafter designated vHNF1-IOSE #1 and #2) express a 62-kDa vHNF1 protein not expressed by mock-transfected hTERT-IOSE (hereafter designated Mock-IOSE; Figure 5*A*). By phase-contrast microscopy, vHNF1-IOSE #2, which represents a clone grown *in vitro* for longer time than vHNF1-IOSE #1 cell line, appeared to lose the typical mesenchymal morphology, whereas both Mock- and vHNF1-IOSE #1 maintained a more spindle-like morphology (Figure 5*B*).

By quantitative RT-PCR on total RNA, the E-cadh transcript was slightly detectable in all transfected IOSE (data not shown). Expression of Snail transcript in vHNF1-expressing clones was found to be downregulated 3- and 4-fold, and Slug transcript 2.5- and 3.5-fold, respectively (Figure 5*C*).

We then analyzed the effect of vHNF1 loss-of-function on the *Cdh1* promoter activity in Mock and vHNF1-IOSE cells (Figure 5*D*) by transiently transfecting the promoter constructs (shown in Figure 4*B*). Luciferase reporter assay showed that the activity of the E-box–containing wt *Cdh1* promoter increased approximately 2.5-fold in vHNF1-IOSE cells in comparison to Mock-IOSE cells. The activities of the mutated E-box1-3-4 construct was approximately twofold de-repressed in vHNF1-IOSE cells compared to Mock-IOSE, suggesting that E-boxes 1, 3, and 4 are relevant for the *CDH1* gene transcription in this type of cells.

These results together demonstrate that vHNF1 negatively regulates specific E-box–binding repressors in normal ovarian cells, which is in line with the data on ovarian carcinoma cells reported above.

vHNF1 Modulates the Proliferative Potential of Ovarian Cancer and Normal Cells

We aimed also to evaluate vHNF1-dependent growth potential in both DNvHNF1 and vHNF1-transfected-IOSE. In culture, DNvHNF1 cells grew slower than Mock cells, so that the DNvHNF1

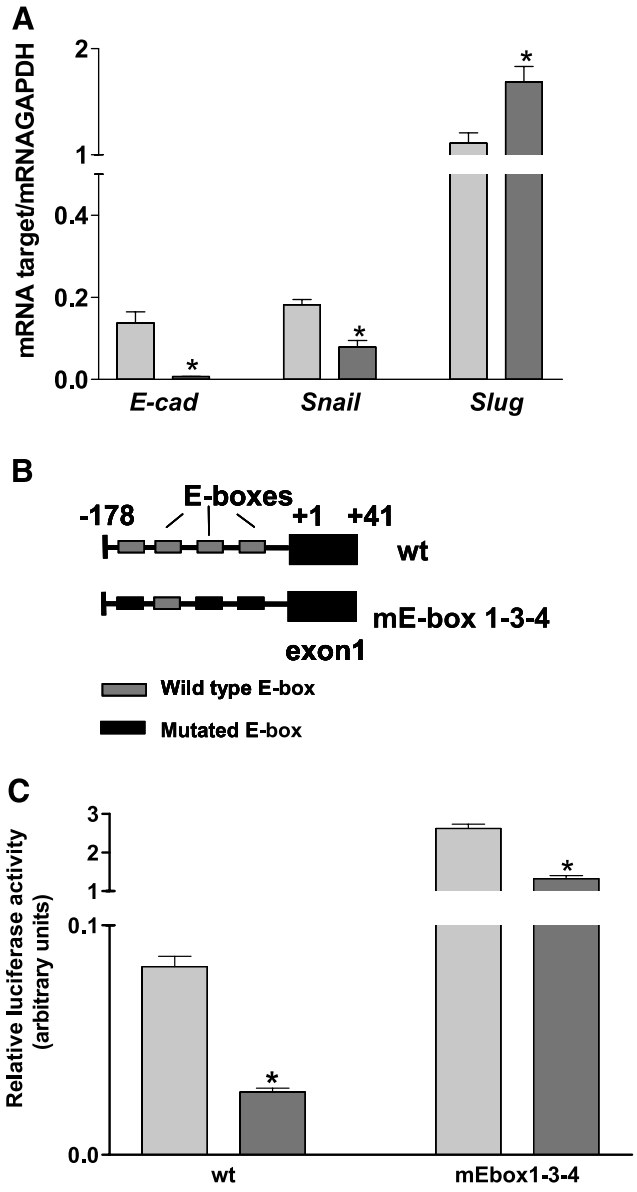

Figure 4. vHNF1 loss-of-function leads to Slug expression and functionality. (A) Quantitative RT-PCR for E-cadh, Snail, and Slug transcripts was performed on total RNA extracted from Mock (light gray bars) and DNvHNF1 (dark gray bars). Data represent mean (SD) for the genes indicated, after normalization to the housekeeping gene *GAPDH* in at least six determinations. Asterisks indicate significant differences ($P \leq .02$). (B) Schematic representation of *Chd1* proximal promoter containing four putative E-box sequences cloned upstream of the *luciferase* gene and transiently transfected in Mock and DNvHNF1 cells. Mutations within the E-boxes are as indicated. (C) Luciferase-promoter gene assay of Mock (light gray bars) and DNvHNF1 (dark gray bars) cells transiently transfected with reporter plasmids containing the wt *Cdh1* proximal promoter or the same promoter with mutated E-box sequences (mEbox) as reported in panel B. Data are mean (SD) normalized for transfection efficiency in three independent experiments performed in triplicate. Asterisk indicates a significant difference ($P \leq .01$).

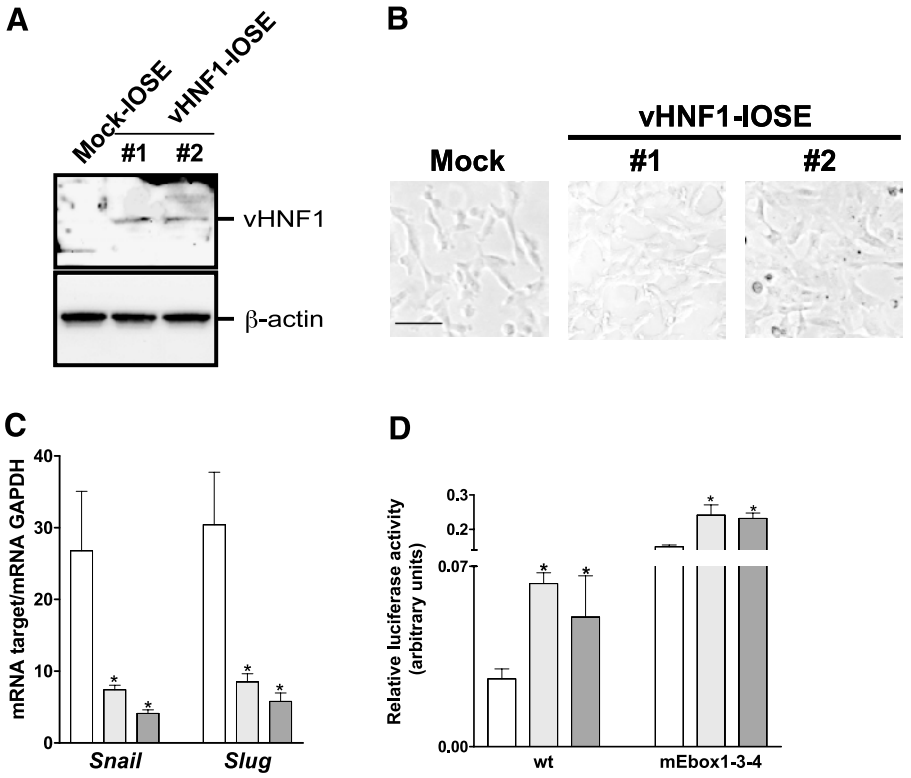

Figure 5. Ectopic expression of vHNF1 in IOSE cells is sufficient to induce Snail and Slug. (A) Western blot analysis of total cell lysates from Mock and DNvHNF1-IOSE clones #1 and #2 was performed with a rabbit anti-vHNF1 Ab. (B) Morphology of Mock and DNvHNF1-IOSE cells. While Mock- and vHNF1-IOSE #1 showed a more spindle-like morphology, vHNF1-IOSE #2, which represents a clone grown *in vitro* for longer time than vHNF1-IOSE #1 cell line, appeared larger in size acquiring a more compacted morphology. Images were obtained by phase-contrast microscopy using a 10× objective. Bar, 100 μm. (C) Quantitative RT-PCR for Snail and Slug transcripts was performed on total RNA extracted from Mock (white bar) and vHNF1-IOSE #1 (light gray bars) and #2 (dark gray bars) cells. Data represent mean (SD) for the relevant genes normalized to the housekeeping gene *GAPDH* in at least six determinations. Asterisks indicate significant differences ($P \leq .05$). (D) Luciferase-promoter gene assay using Mock (white bar) and DNvHNF1-IOSE #1 (light gray bars) and #2 (dark gray bars) cells transiently transfected with promoter reporter plasmids containing the wt *Cdh1* proximal promoter or the same promoter with mutations in the E-box sequences (mEbox) as reported in Figure 4*B*.

cell density was 30% lower on day 5 after seeding ($P = .0001$; Figure 6*A*), consistent with the decrease in proliferation after transient vHNF1 silencing (Figure 1*C*). The slower growth rate was paralleled by reduced colony-forming capability (data not shown).

Growth potential was also evaluated in the IOSE transfected cells up to 7 days. It is noteworthy that ectopic vHNF1 expression caused a two- and three-fold increase of the growth rate of vHNF1-IOSE #1 and #2, respectively, in comparison to Mock-IOSE cells (Figure 6*B*).

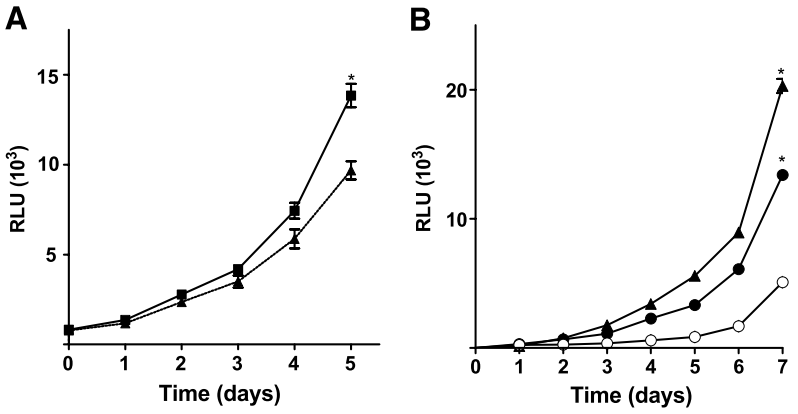

Figure 6. vHNF1 modulates the proliferative potential of ovarian cancer and normal cells. Cells were seeded in 96-well plates, and growth was measured for up to 5 to 7 days with a CellTiter-Glo luminescent cell viability assay kit (Promega). (A) Mock (■) and DNvHNF1 (▲): data represent mean (SD) of six determinations from three independent experiments. (B) Mock (○) and vHNF1-IOSE #1 (●) and #2 (▲): data represent mean (SD) of five determinations from one of three experiments. Asterisks indicate significant differences ($P \leq .05$).

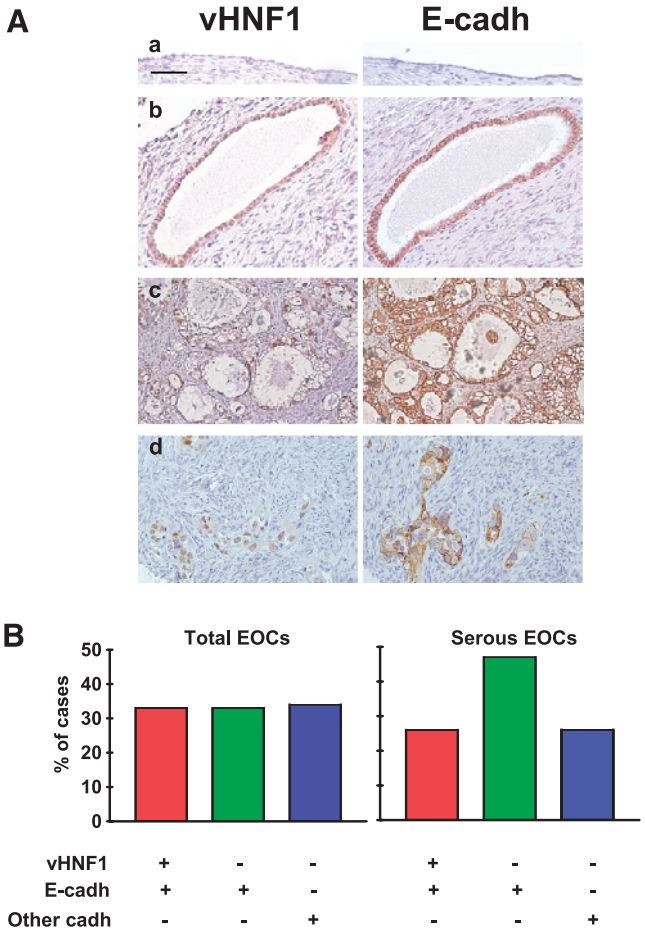

Figure 7. vHNF1 is expressed in a subset of normal and transformed E-cadh–expressing ovarian cells. Immunohistochemical analyses with anti-vHNF1 and –E-cadh Abs on paraffin-embedded normal and tumor-derived ovarian tissues. The immunohistochemical analysis is also reported in Table 2. (A) Representative examples of normal ovarian epithelium (a), an inclusion cyst (b), and two serous EOCs (c and d). Images were obtained with a 20× objective. Bar, 100 μm. (B) Epithelial ovarian carcinomas analyzed for vHNF1 and/or E-cadh expressions. Anti–E-cadh–negative samples comprise other cadh-expressing tumors. Total number of EOCs, n = 38; total number of serous EOCs, n = 19. Vertical bars, percentage of immunoreactive samples.

These results are in line with those shown above (Figure 1*A*) and suggest a positive involvement of vHNF1 in controlling the proliferation of normal and transformed ovarian cells.

vHNF1 Is Expressed in a Subset of Normal and Transformed E-cadh–Expressing Ovarian Cells

We previously showed that vHNF1 is expressed only in ovarian carcinoma cell lines and not in short-term cultures of OSE cells [22]. Here, we used IHC to evaluate vHNF1 expression together with E-cadh in sections from four normal human ovaries, selected for having a normal monolayer epithelium or for presenting invaginations and inclusion cysts lined by a single layer of cells, and in samples from benign, low malignant potential (LMP) and malignant ovarian tumors of different histotypes (Figure 7). When detected, anti-vHNF1 staining was observed only in the nucleus or in the nucleus and the cytoplasm, whereas anti–E-cadh mainly stained the cell membrane. No vHNF1 expression was detected in OSE from different individuals. In 20% of cysts, the single, normal cell layer reacted with anti-vHNF1 together with anti–E-cadh (representative example in Figure 7). Cells from four benign tumors and four of six LMP tumors stained for vHNF1 and E-cadh (Table 2). One LMP tumor that did not stain with anti-vHNF1 was endometrioid. Among the 38 carcinomas tested, 18 reacted with anti-vHNF1: 7 of these were clear cell carcinomas, 5 were serous (representative examples in Figure 7*A*), and 1 was mucinous. Four of 7 endometrioid EOCs were vHNF1-positive.

Interestingly, 66% of EOCs tested were reactive with anti–E-cadh monoclonal Ab, and within these EOCs, 33% were positive for both vHNF1 and E-cadh (Figure 7*B*). Within serous histotype, which represents most EOCs, 73% expressed E-cadh and 26% together with vHNF1. Note that E-cadh–negative tumors could express N-cadh or cadh-11, as previously reported [23].

In conclusion, vHNF1 appears to be expressed in inclusion cysts, and it is clearly expressed in clear cell carcinomas and in some serous carcinomas, but it is not expressed in OSE. Interestingly, vHNF1 expression is significantly associated with E-cadh expression in a subset of samples comprising some cysts as well as in benign and malignant tumors of serous or clear cell histotype, whereas no coexpression was observed in endometrioid tumors (P = .0024).

Discussion

Here, we demonstrate that vHNF1 may act as an initial regulator of OSE plasticity and proliferation, thereby contributing significantly to the changes in differentiation of OSE cells during neoplastic transformation and progression. Indeed, a DN form of the transcription factor vHNF1 induces EMT when expressed in an ovarian carcinoma cell line (SKOV3), as confirmed by a change in mRNA expression profile resembling that of EMT and by a loss at the protein level of E-cadh and components of tight junctions. DNvHNF1 expression in SKOV3 ovarian carcinoma cells downregulated Slug expression and functionality, and conversely, vHNF1 ectopically expressed in hTERT-IOSE cells decreased Snail and Slug expression and functionality. Overall, our results uncover a novel role of vHNF1 in the epithelial differentiation of ovary cells.

The HNF transcription factors have been related mainly to hepatocyte and pancreatic β-cell differentiation, and vHNF1 in particular seems to be required for maintenance of the differentiation state and functional activity of mouse pancreatic β-cells. Mutations and/or deletions that impair vHNF1 functionality cause major alterations in

Table 2. Expression of vHNF1 and E-cadh Detected by Immunohistochemistry in Ovarian Tumor Samples.

Ovarian Tumors*	No. of Cases (n = 49)	Presence of vHNF1/E-cadh by IHC			
		+/+	+/–	–/+	–/–
Benign	5	4	—	1	—
LMP	6	4	—	1	1†
Carcinoma‡:					
Serous	19	5	1	9	4
Mucinous	2	1	—	1	—
Clear cell	10	7	1	—	2
Endometrioid	7	—	3	3	1

*Commercially available tissue arrays.
†Endometrioid LMP tumor.
‡Mucinous and endometrioid carcinomas comprise a grade I tumor; all other carcinomas were grades II and III.

expression of important metabolic genes. Indeed, vHNF1 knock-out mice die within a few days after gastrulation [19]. In adult mice, β-cells show impaired glucose tolerance and reduced insulin secretion when vHNF1 is selectively deleted using *Cre* recombinase [36]. The present results suggest for the first time that vHNF1 is one of the transcription factors governing the epithelial differentiation of OSE.

To evaluate the molecular signature associated with vHNF1 loss-of-function in SKOV3 cells, we performed an EMT-guided comparative expression profile analysis on the basis of a newly compiled EMT-related gene database (Table W1). The observed profile is in agreement with an EMT shift, with a few remarkable exceptions, such as down-modulation of *FN1*, *ID1*, and *ID4* and up-regulation of *ITGB6* and *SEMA3C*. This could simply be caused by cell line specificity of these molecules. Note that vHNF1 loss-of-function does not completely revert the malignancy of SKOV3 cells and that further analysis is needed to determine whether particular molecular mechanisms regulate the expression of these genes in a tumor type–specific way. Conversely, several genes characteristic of either EMT or MET but not yet associated with EOCs were identified as differentially expressed. Microarray and immunofluorescence analyses showed that vHNF1 functionality was associated mainly with genes that modulate cell adhesion and are ECM-related, which is consistent with a role for HNF transcription factors in regulating cell adhesion [37]. The potential usefulness of this information in the context of clinical screening markers and possible genetic or pharmacologic targeting awaits further validation of the role of vHNF1 and the newly identified associated genes, together with detailed gene expression comparisons between OSE and EOC samples.

Consistent with a previous report that only EOC with clear cell histotype expresses vHNF1 [38], our immunohistochemical analysis revealed vHNF1 expression in most clear cell EOCs, as well as in approximately 30% of serous EOCs, which are most EOCs. We detected heterogeneous expression of vHNF1 associated to E-cadh expression in 32% of the EOC samples, independently of tumor grading. These results confirm a role for vHNF1 in the epithelial phenotype of EOCs. An analysis to define the molecular signature that characterizes this subset of EOCs, which include mainly the clear cell and serous histotypes, is ongoing.

Previous studies indicated that the proximal vHNF1 promoter was methylated in 26% of the EOCs analyzed, but no such methylation was observed in OSE cells that do not express vHNF1 [39]. In renal cell carcinomas, *TCF2* inactivation was caused by germ line mutations [17]. Therefore, in vHNF1-negative ovarian carcinomas, *TCF2* gene could have either methylated promoter or inactivating mutations. We further hypothesize that cysts undergo transformation if they contain genetic mutations and possibly express vHNF1 conferring a further growth advantage. Epithelial ovarian carcinomas derived from those cysts continue to express vHNF1, but once tumors progress, epigenetic mechanisms such as methylation of the vHNF1 promoter might be activated, resulting in loss of vHNF1 expression. One key function of vHNF1 seems to be the negative modulation of EMT-inducing transcription factors such as Snail and Slug, leading to the positive modulation of E-cadh and other epithelial proteins. Previously, vHNF1 has been shown to be involved in MET occurring during kidney development, whereas kidney fibrosis has been associated with the binding of the E-box–binding repressors Snail or Slug to the promoters of vHNF1 and E-cadh encoding genes [40]. These results together with ours favor the hypothesis of a delicate reciprocal transcriptional regulation between E-box repressors and vHNF1. Recently, another embryonic transcription factor, FOXC2, was identified as a central modulator of the EMT program in metastatic basal-like breast cancer [41]. These observations, together with ours, support the hypothesis that embryonic transcription factors are necessary for execution of transformation or invasion programs in different types of cancers. Of course, this hypothesis does not exclude that other mechanisms, such as those involving specific HOX genes, might contribute to determining the morphologic heterogeneity of EOCs [42].

In addition to its role in OSE cell plasticity, vHNF1 seems to contribute to the increased growth potential of normal and transformed ovarian cells. Indeed, siRNA-mediated silencing of vHNF1 or its inhibition by a DN mutant was associated with decreased growth proliferation, whereas *de novo* expression of vHNF1 increased proliferation. The increase in proliferation could be attributed to the modulation of cell cycle progression but did not confer unlimited growth potential to OSE cells (unpublished observation). We can also hypothesize that the vHNF1 confers a growth advantage *in vitro* so that ovarian carcinoma cell lines maintain vHNF1 expression, whereas in tumors the genomic modifications described above lead to the loss of vHNF1 expression.

Recently, a new model for the pathogenesis of EOCs has been proposed in which ovarian tumors are divided in two types [43]. Type I tumors, which include low-grade serous, mucinous, endometrioid, and clear cell carcinomas, are slowly growing and are generally confined to the ovary. Type II tumors are rapidly growing and highly aggressive. Despite considerable efforts, it is not yet possible to distinguish these different types of ovarian tumors at early stage and set up the most successful therapy. In this context, the strong association of vHNF1 with E-cadh in clear cell and in a subset of serous carcinomas could potentially contribute in distinguishing different types of ovarian tumors, on a more extensive molecular analysis. Epithelial-mesenchymal transition has been recognized as a potential mechanism for carcinoma progression. The mechanisms governing EMT in tumor progression recapitulate many of those identified in embryogenesis [10–12]. However, besides EOC with endometrioid histotype, EOCs seem to diverge in other ways from the general EMT scenario. For example, β-ctn does not detectably activate β-ctn/TCF-responsive genes on progression [44], whereas E-cadh expression is maintained in advanced EOCs [6,45]. Therefore, increasing knowledge of the molecular mechanisms of MET occurring at first stages of tumorigenesis and controlled by vHNF1 in EOCs may provide new and fascinating insights into the biology of this important disease and likely to identifying early detection markers and to opening potential avenues for therapeutic intervention.

Acknowledgments

The authors thank M.L. Sensi and A. Bredan for critical reading of the article and Gloria Bosco for her secretarial assistance.

References

[1] Shih IeM and Kurman RJ (2004). Ovarian tumorigenesis: a proposed model based on morphological and molecular genetic analysis. *Am J Pathol* **164**, 1511–1518.

[2] Bell DA (2005). Origins and molecular pathology of ovarian cancer. *Mod Pathol* **18** (Suppl 2), S19–S32.

[3] Auersperg N, Wong AS, Choi KC, Kang SK, and Leung PC (2001). Ovarian surface epithelium: biology, endocrinology, and pathology. *Endocr Rev* **22**, 255–288.

[4] Strumane K, Van Roy F, and Berx G (2003). The role of E-cadherin in epithelial differentiation and cancer progression. *Recent Res Devel Cell Biochem* **1**, 33–37.

[5] Richmond PJM, Karayiannakis AJ, Nagafuchi A, Kaisary AV, and Pignatelli M (1997). Aberrant E-cadherin and α-catenin expression in prostate cancer: correlation with patient survival. *Cancer Res* **57**, 3189–3193.

[6] Sundfeldt K (2003). Cell-cell adhesion in the normal ovary and ovarian tumors of epithelial origin; an exception to the rule. *Mol Cell Endocrinol* **202**, 89–96.

[7] Auersperg N, Pan J, Grove BD, Peterson T, Fisher J, Maines-Bandiera S, Somasiri A, and Roskelley CD (1999). E-cadherin induces mesenchymal-to-epithelial transition in human ovarian surface epithelium. *Proc Natl Acad Sci USA* **96**, 6249–6254.

[8] Maines-Bandiera SL, Huntsman D, Lestou VS, Kuo WL, Leung PC, Horsman RD, Wong AS, Woo MM, Choi KK, Roskelley CD, et al. (2004). Epithelio-mesenchymal transition in a neoplastic ovarian epithelial hybrid cell line. *Differentiation* **72**, 150–161.

[9] Huber MA, Kraut N, and Beug H (2005). Molecular requirements for epithelial-mesenchymal transition during tumor progression. *Curr Opin Cell Biol* **17**, 548–558.

[10] Thiery JP and Sleeman JP (2006). Complex networks orchestrate epithelial-mesenchymal transitions. *Nat Rev Mol Cell Biol* **7**, 131–142.

[11] Thompson EW, Newgreen DF, and Tarin D (2005). Carcinoma invasion and metastasis: a role for epithelial-mesenchymal transition? *Cancer Res* **65**, 5991–5995.

[12] Savagner P (2005). *Rise and Fall of Epithelial Phenotype: Concept of Epithelial-Mesenchymal Transition*. Landes Bioscience Ed., Kluwer Academic/Plenum Publishers, New York, NY.

[13] Peinado H, Olmeda D, and Cano A (2007). Snail, Zeb and bHLH factors in tumour progression: an alliance against the epithelial phenotype? *Nat Rev Cancer* **7**, 415–428.

[14] Pontoglio M (2000). Hepatocyte nuclear factor 1, a transcription factor at the crossroads of glucose homeostasis. *J Am Soc Nephrol* **11** (Suppl 16), S140–S143.

[15] Bluteau O, Jeannot E, Bioulac-Sage P, Marques JM, Blanc JF, Bui H, Beaudoin JC, Franco D, Balabaud C, Laurent-Puig P, et al. (2002). Bi-allelic inactivation of TCF1 in hepatic adenomas. *Nat Genet* **32**, 312–315.

[16] Rebouissou S, Rosty C, Lecuru F, Boisselier S, Bui H, Frere-Belfa MA, Sastre X, Laurent-Puig P, and Zucman-Rossi J (2004). Mutation of TCF1 encoding hepatocyte nuclear factor 1alpha in gynecological cancer. *Oncogene* **23**, 7588–7592.

[17] Rebouissou S, Vasiliu V, Thomas C, Bellanne-Chantelot C, Bui H, Chretien Y, Timsit J, Rosty C, Laurent-Puig P, Chauveau D, et al. (2005). Germline hepatocyte nuclear factor 1alpha and 1beta mutations in renal cell carcinomas. *Hum Mol Genet* **14**, 603–614.

[18] Gudmundsson J, Sulem P, Steinthorsdottir V, Bergthorsson JT, Thorleifsson G, Manolescu A, Rafnar T, Gudbjartsson D, Agnarsson BA, Baker A, et al. (2007). Two variants on chromosome 17 confer prostate cancer risk, and the one in TCF2 protects against type 2 diabetes. *Nat Genet* **39**, 977–983.

[19] Haumaitre C, Barbacci E, Jenny M, Ott MO, Gradwohl G, and Cereghini S (2005). Lack of TCF2/vHNF1 in mice leads to pancreas agenesis. *Proc Natl Acad Sci USA* **102**, 1490–1495.

[20] Gresh L, Fischer E, Reimann A, Tanguy M, Garbay S, Shao X, Hiesberger T, Fiette L, Igarashi P, Yaniv M, et al. (2004). A transcriptional network in polycystic kidney disease. *EMBO J* **23**, 1657–1668.

[21] Barbacci E, Reber M, Ott MO, Breillat C, Huetz F, and Cereghini S (1999). Variant hepatocyte nuclear factor 1 is required for visceral endoderm specification. *Development* **126**, 4795–4805.

[22] David KA, Milowsky MI, Kostakoglu L, Vallabhajosula S, Goldsmith SJ, Nanus DM, and Bander NH (2006). Clinical utility of radiolabeled monoclonal antibodies in prostate cancer. *Clin Genitourin Cancer* **4**, 249–256.

[23] De Cecco L, Marchionni L, Gariboldi M, Reid JF, Lagonigro MS, Caramuta S, Ferrario C, Bussani E, Mezzanzanica D, Turatti F, et al. (2004). Gene expression profiling of advanced ovarian cancer: characterization of molecular signature involving the fibroblast growth factor 2. *Oncogene* **23**, 8171–8183.

[24] Sanna E, Miotti S, Mazzi M, De Santis G, Canevari S, and Tomassetti A (2007). Binding of nuclear caveolin-1 to promoter elements of growth-associated genes in ovarian carcinoma cells. *Exp Cell Res* **313**, 1307–1317.

[25] Bagnoli M, Tomassetti A, Figini M, Flati S, Dolo V, Canevari S, and Miotti S (2000). Downmodulation of caveolin-1 expression in human ovarian carcinoma is directly related to a-folate receptor overexpression. *Oncogene* **19**, 4754–4763.

[26] Jechlinger M, Grunert S, Tamir IH, Janda E, Ludemann S, Waerner T, Seither P, Weith A, Beug H, and Kraut N (2003). Expression profiling of epithelial plasticity in tumor progression. *Oncogene* **22** (46), 7155–7169.

[27] Moreno-Bueno G, Cubillo E, Sarrio D, Peinado H, Rodriguez-Pinilla SM, Villa S, Bolos V, Jorda M, Fabra A, Portillo F, et al. (2006). Genetic profiling of epithelial cells expressing E-cadherin repressors reveals a distinct role for Snail, Slug, and E47 factors in epithelial-mesenchymal transition. *Cancer Res* **66**, 9543–9556.

[28] Castellano G, Reid JF, Alberti P, Carcangiu ML, Tomassetti A, and Canevari S (2006). New potential ligand-receptor signaling loops in ovarian cancer identified in multiple gene expression studies. *Cancer Res* **66**, 10709–10719.

[29] Janda E, Nevolo M, Lehmann K, Downward J, Beug H, and Grieco M (2006). Raf plus TGFbeta-dependent EMT is initiated by endocytosis and lysosomal degradation of E-cadherin. *Oncogene* **25**, 7117–7130.

[30] Barbacci E, Chalkiadaki A, Masdeu C, Haumaitre C, Lokmane L, Loirat C, Cloarec S, Talianidis I, Bellanne-Chantelot C, and Cereghini S (2004). HNF1beta/TCF2 mutations impair transactivation potential through altered co-regulator recruitment. *Hum Mol Genet* **13**, 3139–3149.

[31] Gottardi CJ, Arpin M, Fanning AS, and Louvard D (1996). The junction-associated protein, zonula occludens-1, localizes to the nucleus before the maturation and during the remodeling of cell-cell contacts. *Proc Natl Acad Sci USA* **93**, 10779–10784.

[32] Traweger A, Fuchs R, Krizbai IA, Weiger TM, Bauer HC, and Bauer H (2003). The tight junction protein ZO-2 localizes to the nucleus and interacts with the heterogeneous nuclear ribonucleoprotein scaffold attachment factor-B. *J Biol Chem* **278**, 2692–2700.

[33] Tronche F, Ringeisen F, Blumenfeld M, Yaniv M, and Pontoglio M (1997). Analysis of the distribution of binding sites for a tissue-specific transcription factor in the vertebrate genome. *J Mol Biol* **266**, 231–245.

[34] Heinzelmann-Schwarz VA, Gardiner-Garden M, Henshall SM, Scurry J, Scolyer RA, Davies MJ, Heinzelmann M, Kalish LH, Bali A, Kench JG, et al. (2004). Overexpression of the cell adhesion molecules DDR1, Claudin 3, and Ep-CAM in metaplastic ovarian epithelium and ovarian cancer. *Clin Cancer Res* **10**, 4427–4436.

[35] Lee JM, Dedhar S, Kalluri R, and Thompson EW (2006). The epithelial-mesenchymal transition: new insights in signaling, development, and disease. *J Cell Biol* **172**, 973–981.

[36] Wang L, Coffinier C, Thomas MK, Gresh L, Eddu G, Manor T, Levitsky LL, Yaniv M, and Rhoads DB (2004). Selective deletion of the Hnf1beta (*MODY5*) gene in beta-cells leads to altered gene expression and defective insulin release. *Endocrinology* **145**, 3941–3949.

[37] Battle MA, Konopka G, Parviz F, Gaggl AL, Yang C, Sladek FM, and Duncan SA (2006). Hepatocyte nuclear factor 4alpha orchestrates expression of cell adhesion proteins during the epithelial transformation of the developing liver. *Proc Natl Acad Sci USA* **103**, 8419–8424.

[38] Kato N, Sasou S, and Motoyama T (2006). Expression of hepatocyte nuclear factor-1beta (HNF-1beta) in clear cell tumors and endometriosis of the ovary. *Mod Pathol* **19**, 83–89.

[39] Terasawa K, Toyota M, Sagae S, Ogi K, Suzuki H, Sonoda T, Akino K, Maruyama R, Nishikawa N, Imai K, et al. (2006). Epigenetic inactivation of TCF2 in ovarian cancer and various cancer cell lines. *Br J Cancer* **94**, 914–921.

[40] Boutet A, De Frutos CA, Maxwell PH, Mayol MJ, Romero J, and Nieto MA (2006). Snail activation disrupts tissue homeostasis and induces fibrosis in the adult kidney. *EMBO J* **25**, 5603–5613.

[41] Mani SA, Yang J, Brooks M, Schwaninger G, Zhou A, Miura N, Kutok JL, Hartwell K, Richardson AL, and Weinberg RA (2007). Mesenchyme Forkhead 1 (FOXC2) plays a key role in metastasis and is associated with aggressive basal-like breast cancers. *Proc Natl Acad Sci USA* **104**, 10069–10074.

[42] Cheng W, Liu J, Yoshida H, Rosen D, and Naora H (2005). Lineage infidelity of epithelial ovarian cancers is controlled by HOX genes that specify regional identity in the reproductive tract. *Nat Med* **11**, 531–537.

[43] Kurman RJ and Shih IeM (2008). Pathogenesis of ovarian cancer: lessons from morphology and molecular biology and their clinical implications. *Int J Gynecol Pathol* **27**, 151–160.

[44] Wu R, Zhai Y, Fearon ER, and Cho KR (2001). Diverse mechanisms of beta-catenin deregulation in ovarian endometrioid adenocarcinomas. *Cancer Res* **61**, 8247–8255.

[45] Ahmed N, Thompson EW, and Quinn MA (2007). Epithelial-mesenchymal interconversions in normal ovarian surface epithelium and ovarian carcinomas: an exception to the norm. *J Cell Physiol* **213**, 581–588.

Table W1. List of EMT-Related Genes.

Gene Symbol	Name	Gene ID
Epithelial genes		
Actin cytoskeleton organization		
ARHGAP5	Rho GTPase activating protein 5	394
ARHGDIA	Rho GDP dissociation inhibitor (GDI) alpha	396
ARHGEF1	Rho guanine nucleotide exchange factor (GEF) 1	9138
DST	Dystonin	667
FLNA	Filamin A, alpha (actin binding protein 280)	2316
PODXL	Podocalyxin-like	5420
Apoptosis		
CTNNAL1	Catenin (cadherin-associated protein), alpha-like 1	8727
MAP3K5	Mitogen-activated protein kinase kinase kinase 5	4217
PRKCZ	Protein kinase C, zeta	5590
SGK	Serum/glucocorticoid–regulated kinase	6446
Cell adhesion and/or ECM-related		
ANXA4	Annexin A4	307
CD99	CD99 molecule	4267
CDH1	Cadherin 1, type 1, E-cadherin (epithelial)	999
CDH16	Cadherin 16, KSP-cadherin	1014
CLDN1	Claudin 1	9076
CLDN7	Claudin 7	1366
DSG2	Desmoglein 2	1829
EVA1	Epithelial V–like antigen 1	10205
FBLP-1	filamin binding LIM protein 1	54751
ILK	Integrin-linked kinase	3611
ITGA3	Integrin, alpha 3 (antigen CD49C, alpha 3 subunit of VLA-3 receptor)	3675
ITGA5	Integrin, alpha 5 (fibronectin receptor, alpha polypeptide)	3678
ITGB1	Integrin, beta 1	3688
ITGB5	Integrin, beta 5	3693
ITGB6	Integrin, beta 6	3694
JUP	Junction plakoglobin	3728
KITLG	KIT ligand	4254
LAMA3	Laminin, alpha 3	3909
MAP17	membrane-associated protein 17	10158
NID2	Nidogen 2 (osteonidogen)	22795
NRP2	Neuropilin 2	8828
OCLN	Occludin	4950
PKP1	Plakophilin 1 (ectodermal dysplasia/skin fragility syndrome)	5317
SCRIB	Scribbled homolog (*Drosophila*)	23513
Cell cycle		
CCND1	Cyclin D1	595
CDK7	Cyclin-dependent kinase 7 (MO15 homolog, *Xenopus laevis*, cdk-activating kinase)	1022
DUSP1	Dual specificity phosphatase 1	1843
HDAC3	Histone deacetylase 3	8841
MAFG	V-*maf* musculoaponeurotic fibrosarcoma oncogene homolog G (avian)	4097
SFN	Stratifin	2810
PLK2	Polo-like kinase 2	10769
TOB2	Transducer of ERBB2, 2	10766
YES1	V-yes-1 Yamaguchi sarcoma viral oncogene homolog 1	7525
Cell growth and/or maintenance		
ATP1A1	ATPase, Na^+/K^+ transporting, alpha 1 polypeptide	476
ATP1A3	ATPase, Na^+/K^+ transporting, alpha 3 polypeptide	478
ATP1B1	ATPase, Na^+/K^+ transporting, beta 1 polypeptide	481
BCL6	B-cell CLL/lymphoma 6 (zinc finger protein 51)	604
BMP4	Bone morphogenetic protein 4	652
BPAG1	Hemidesmosomal plaque protein	667
BTG2	BTG family, member 2	7832
CTGF	Connective tissue growth factor	1490
DAB2	Disabled homolog 2, mitogen-responsive phosphoprotein (*Drosophila*)	1601
DEFB1	Defensin, beta 1	1672
FABP1	Fatty acid binding protein 1, liver	2168
FOS	V-*fos* FBJ murine osteosarcoma viral oncogene homolog	2353
FOSB	FBJ murine osteosarcoma viral oncogene homolog B	2354
GAB1	GRB2-associated binding protein 1	2549
GC	Group-specific component (vitamin D binding protein)	2638
GDI2	GDP dissociation inhibitor 2	2665
GPC3	Glypican 3	2719
GRB7	Growth factor receptor–bound protein 7	2886
HBP17	Fibroblast growth factor binding protein 1	9982
HDGF	Hepatoma-derived growth factor (high-mobility group protein 1-like)	3068
ITPR1	Inositol 1,4,5-triphosphate receptor, type 1	3708
KRT14	Keratin 14	3861
KRT19	Keratin 19	3880
KRT8	Keratin 8	3856
MST1R	Macrophage stimulating 1 receptor (c-*met*–related tyrosine kinase)	4486
MUC1	Mucin 1, cell surface associated	4582
NET1	Neuroepithelial cell transforming gene 1	10276
NNT	Nicotinamide nucleotide transhydrogenase	23530
PROCR	Protein C receptor, endothelial (EPCR)	10544
PTPN1	Protein tyrosine phosphatase, non–receptor type 1	5770
RARA	Retinoic acid receptor, alpha	5914
RGS2	Regulator of G-protein signaling 2, 24 kDa	5997
SEMA3C	Sema domain, immunoglobulin domain (Ig), short basic domain, secreted, (semaphorin) 3C	10512
SMARCC1	SWI/SNF–related, matrix-associated	6599
SRF	Serum response factor (c-*fos* serum response element–binding transcription factor)	6722
STAT5A	Signal transducer and activator of transcription 5A	6776
TACSTD1	Tumor-associated calcium signal transducer 1	4072
TACSTD2	Tumor-associated calcium signal transducer 2	4070
TCF3	Transcription factor 3 (E2A immunoglobulin enhancer binding factors E12/E47)	6929
TGFB3	Transforming growth factor, beta 3	7043
TGM2	Transglutaminase 2 (C polypeptide, protein-glutamine-gamma-glutamyltransferase)	7052
TJP1	Tight junction protein 1 (zona occludens 1)	7082
TSC22D1	TSC22 domain family, member 1	8848
VAMP8	Vesicle-associated membrane protein 8 (endobrevin)	8673
Cell motility		
ACTN4	Actinin, alpha 4	81
F11R	F11 receptor	50848
HMMR	Hyaluronan-mediated motility receptor (RHAMM)	3161
JAG1	Jagged 1 (Alagille syndrome)	182
SERPINB5	Serpin peptidase inhibitor, clade B (ovalbumin), member 5	5268
SPP1	Secreted phosphoprotein 1 (osteopontin, bone sialoprotein I)	6696
THBS1	Thrombospondin 1	7057
TIAM1	T-cell lymphoma invasion and metastasis 1	7074
Development and/or differentiation		
DSP	Desmoplakin	1832
EGR2	Early growth response 2 (Krox-20 homolog, *Drosophila*)	1959
FGF13	Fibroblast growth factor 13	2258
GATA3	GATA binding protein 3	2625
GATA4	GATA binding protein 4	2626
GATA6	GATA binding protein 6	2627
HELLS	Helicase, lymphoid-specific	3070
HNF4A	Hepatocyte nuclear factor 4, alpha	3172
INHBB	Inhibin, beta B (activin AB beta polypeptide)	3625
MITF	Microphthalmia-associated transcription factor	4286
MSX2	Msh homeobox 2	4488
NUMB	Numb homolog (*Drosophila*)	8650
SCEL	Sciellin	8796
TCF4	Transcription factor 4	6925
TCF6	Transcription factor 6–like	7019
TGIF	TGFB-induced factor (TALE family homeobox)	7050
Metabolism		
AMD1	Adenosylmethionine decarboxylase 1	262
ATF3	Activating transcription factor 3	467
CA2	Carbonic anhydrase II	760
CHKA	Choline kinase alpha	1119
CITED2	Cbp/p300–interacting transactivator, with Glu/Asp–rich carboxy-terminal domain, 2	10370
CTSH	Cathepsin H	1512
CYP1A1	Cytochrome P450, family 1, subfamily A, polypeptide 1	1543
EGR1	Early growth response 1	1958
EXT1	Exostoses (multiple) 1	2131

Table W1. (*continued*)

Gene Symbol	Name	Gene ID
FBP2	Fructose-1,6-bisphosphatase 2	8789
INMT	Indolethylamine *N*-methyltransferase	11185
IRF6	Interferon regulatory factor 6	3664
KLF2	Kruppel-like factor 2 (lung)	10365
LMO7	LIM domain 7	4008
NR4A1	Nuclear receptor subfamily 4, group A, member 1	3164
PADI2	Peptidyl arginine deiminase, type II	11240
PC	Pyruvate carboxylase	5091
PFTK1	PFTAIRE protein kinase 1	5218
POLR2A	Polymerase (RNA) II (DNA directed) polypeptide A, 220 kDa	5430
PTK9	protein tyrosine kinase 9	5756
SERPINB6	Serpin peptidase inhibitor, clade B (ovalbumin), member 6	5269
SFRS4	Splicing factor, arginine/serine–rich 4	6429
SP2	Sp2 transcription factor	6668
TCF1	Transcription factor 1, hepatic; LF-B1, hepatic nuclear factor (HNF1), albumin proximal factor	6927
TCF2	Transcription factor 2, hepatic; LF-B3; variant hepatic nuclear factor	6928
TIMP3	TIMP metallopeptidase inhibitor 3 (Sorsby fundus dystrophy, pseudoinflammatory)	7078
TJP2	Tight junction protein 2 (zona occludens 2)	9414
ZFP36	Zinc finger protein 36, C3H type, homolog (mouse)	7538
ZNF239	Zinc finger protein 239	8187
Mesenchymal genes		
Actin cytoskeleton organization		
ACTG1	Actin, gamma 1	71
ACTN1	Actinin, alpha 1	87
CFL1	Cofilin 1 (nonmuscle)	1072
CORO1C	Coronin, actin binding protein, 1C	23603
FLNB	Filamin B, beta (actin binding protein 278)	2317
PLEK2	Pleckstrin 2	26499
SDC1	Syndecan 1	6382
VIM	Vimentin	7431
WASPIP	WAS/WASL interacting protein family, member 1	7456
Apoptosis		
CASP9	Caspase 9, apoptosis-related cysteine peptidase	842
Cell adhesion and/or ECM-related		
BGN	Biglycan	633
CD44	CD44 molecule (Indian blood group)	960
CDH15	Cadherin 15, M-cadherin (myotubule)	1013
CDH2	Cadherin 2, type 1, N-cadherin	1000
CDH6	Cadherin 6, type 2, K-cadherin (fetal kidney)	1004
COL15A1	Collagen, type XV, alpha 1	1306
COL1A2	Collagen, type I, alpha 2	1278
COL5A1	Collagen, type V, alpha 1	1289
COL5A2	Collagen, type V, alpha 2	1290
COL6A1	Collagen, type VI, alpha 1	1291
COL6A2	Collagen, type VI, alpha 2	1292
CTNND1	Catenin (cadherin-associated protein), delta 1	1500
DDR2	Discoidin domain receptor family, member 2	4921
DLG5	Discs, large homolog 5 (*Drosophila*)	9231
FN1	Fibronectin 1	2335
Lamb1	Laminin, beta 1	3912
LGALS3	Lectin, galactoside-binding, soluble, 3 (galectin 3)	3958
PTPNS1	Protein tyrosine phosphatase, non–receptor type substrate 1	8194
TNC	Tenascin C (hexabrachion)	3371
TNXB	Tenascin XB	7148
VCL	Vinculin	7414
VTN	Vitronectin	7448
Cell cycle		
ABL1	V-*abl* Abelson murine leukemia viral oncogene homolog 1	25
AK1	Adenylate kinase 1	203
BCL3	B-cell CLL/lymphoma 3	602
BTG3	BTG family, member 3	10950
CDC2	Cell division cycle 2, G_1 to S and G_2 to M	983
CDKN1A	Cyclin-dependent kinase inhibitor 1A (p21, Cip1)	1026
CDKN2A	Cyclin-dependent kinase inhibitor 2A (melanoma, p16, inhibits CDK4)	1029
CDKN2C	Cyclin-dependent kinase inhibitor 2C (p18, inhibits CDK4)	1031
GAS1	Growth arrest–specific 1	2619
PSEN2	Presenilin 2 (Alzheimer disease 4)	5664
Cell growth and/or maintenance		
ABCA9	ATP-binding cassette, subfamily A (ABC1), member 9	10350
ABCC11	ATP-binding cassette, subfamily C (CFTR/MRP), member 11	85320
AFP	Alpha-fetoprotein	174
BMP7	Bone morphogenetic protein 7 (osteogenic protein 1)	655
BSG	Basigin (Ok blood group)	682
CAV1	Caveolin 1, caveolae protein, 22 kDa	857
CCK	Cholecystokinin	885
CCL2	Chemokine (C-C motif) ligand 2	6347
CCL8	Chemokine (C-C motif) ligand 8	6355
CD68	CD68 molecule	968
CTGF	Connective tissue growth factor	1490
CXCL1	Chemokine (C-X-C motif) ligand 1 (melanoma growth stimulating activity, alpha)	2919
CXCL5	Chemokine (C-X-C motif) ligand 5	6374
CXCR7	Chemokine (C-X-C motif) receptor 7	57007
EDG1	Endothelial differentiation, sphingolipid G-protein–coupled receptor, 1	1901
EPS8	Epidermal growth factor receptor pathway substrate 8	2059
FZD1	Frizzled homolog 1 (*Drosophila*)	8321
FZD10	Frizzled homolog 10 (*Drosophila*)	11211
FZD2	Frizzled homolog 2 (*Drosophila*)	2535
FZD3	Frizzled homolog 3 (*Drosophila*)	7976
FZD4	Frizzled homolog 4 (*Drosophila*)	8322
FZD5	Frizzled homolog 5 (*Drosophila*)	7855
FZD6	Frizzled homolog 6 (*Drosophila*)	8323
FZD7	Frizzled homolog 7 (*Drosophila*)	8324
FZD8	Frizzled homolog 8 (*Drosophila*)	8325
FZD9	Frizzled homolog 9 (*Drosophila*)	8326
IFI6	Interferon, alpha-inducible protein 6	2537
GBP3	Guanylate binding protein 3	2635
GNAQ	Guanine nucleotide binding protein (G protein), q polypeptide	2776
GNG11	Guanine nucleotide binding protein (G protein), gamma 11	2791
GABBR2	gamma-aminobutyric acid (GABA) B receptor, 2	9568
HGF	Hepatocyte growth factor (hepapoietin A; scatter factor)	3082
HIF1	Hypoxia-inducible factor 1	3091
EPAS1	Hypoxia-inducible factor 2	2034
HMGA2	High mobility group AT-hook 2	8091
IGFBP1	Insulin-like growth factor binding protein 1	3484
IGFBP3	Insulin-like growth factor binding protein 3	3486
IGFBP4	Insulin-like growth factor binding protein 4	3487
IGFBP5	Insulin-like growth factor binding protein 5	3488
IL8RB	Interleukin 8 receptor, beta	3579
KIFAP3	Kinesin-associated protein 3	22920
MADH4	SMAD family member 4	4089
MEIS1	Meis homeobox 1	4211
MET	Met proto-oncogene (hepatocyte growth factor receptor)	4233
MYBBP1A	MYB binding protein (P160) 1a	10514
NTRK3	Neurotrophic tyrosine kinase, receptor, type 3	4916
PCOLCE	Procollagen C-endopeptidase enhancer	5118
PDGFA	Platelet-derived growth factor alpha polypeptide	5154
PDGFRA	Platelet-derived growth factor receptor, alpha polypeptide	5156
PDGFRB	Platelet-derived growth factor receptor, beta polypeptide	5159
PHGDH	Phosphoglycerate dehydrogenase	26227
PKC	Paroxysmal kinesigenic choreoathetosis	50818
PMP22	Peripheral myelin protein 22	5376
PTHLH	Parathyroid hormone–like hormone	5744
PTPN22	Protein tyrosine phosphatase, non–receptor type 22 (lymphoid)	26191
PTPN7	Protein tyrosine phosphatase, non–receptor type 7	5778

Table W1. (*continued*)

Gene Symbol	Name	Gene ID
PTPRM	Protein tyrosine phosphatase, receptor type, M	5797
REL	V-*rel* reticuloendotheliosis viral oncogene homolog (avian)	5966
RRAS	Related RAS viral (r-*ras*) oncogene homolog	6237
SLC29A1	Solute carrier family 29 (nucleoside transporters), member 1	2030
SRC	V-*src* sarcoma (Schmidt-Ruppin A-2) viral oncogene homolog (avian)	6714
STAT1	Signal transducer and activator of transcription 1, 91 kDa	6772
TCF3	Transcription factor 3 (E2A immunoglobulin enhancer binding factors E12/E47)	6929
TCF8	Transcription factor 8 (represses interleukin 2 expression)	6935
TGFB1	Transforming growth factor, beta 1 (Camurati-Engelmann disease)	7040
TIEG	Kruppel-like factor 10	7071
TLN1	Talin 1	7094
TSPAN-3	tetraspanin 3	10099
TUBA6	Tubulin, alpha 6	84790
Cell motility		
ACTB	Actin, beta	60
C4A	complement component 4A	720
CALD1	Caldesmon 1	800
CTSB	Cathepsin B	1508
CTSZ	Cathepsin Z	1522
GRN	Granulin	2896
MMP10	Matrix metallopeptidase 10 (stromelysin 2)	4319
MMP12	Matrix metallopeptidase 12 (macrophage elastase)	4321
MMP13	Matrix metallopeptidase 13 (collagenase 3)	4322
MMP2	Matrix metallopeptidase 2 (gelatinase A, 72 kDa gelatinase, 72 kDa type IV collagenase)	4313
MMP7	Matrix metallopeptidase 7 (matrilysin, uterine)	4316
MMP9	Matrix metallopeptidase 9 (gelatinase B, 92 kDa gelatinase, 92 kDa type IV collagenase)	4318
MSN	Moesin	4478
NOTCH2	Notch homolog 2 (*Drosophila*)	4853
PLA2G7	Phospholipase A2, group VII (platelet-activating factor acetylhydrolase, plasma)	7941
PLAU	Plasminogen activator, urokinase	5328
PLAUR	Plasminogen activator, urokinase receptor	5329
S100A2	S100 calcium binding protein A2	6273
S100A3	S100 calcium binding protein A3	6274
S100A4	S100 calcium binding protein A4	6275
S100A6	S100 calcium binding protein A6	6277
S100A8	S100 calcium binding protein A8	6279
S100P	S100 calcium binding protein P	6286
SERPINH1	Serpin peptidase inhibitor, clade H (heat shock protein 47), member 1	871
TIMP1	TIMP metallopeptidase inhibitor 1	7076
Development and/or differentiation		
COL3A1	Collagen, type III, alpha 1 (Ehlers-Danlos syndrome type IV, autosomal dominant)	1281
CYP1B1	Cytochrome P450, family 1, subfamily B, polypeptide 1	1545
DCN	Decorin	1634
FGF19	Fibroblast growth factor 19	9965
FLOT1	Flotillin 1	10211
ID1	Inhibitor of DNA binding 1, dominant negative helix-loop-helix protein	3397
ID3	Inhibitor of DNA binding 3, dominant negative helix-loop-helix protein	3399
ID4	Inhibitor of DNA binding 4, dominant negative helix-loop-helix protein	3400
IL11	Interleukin 11	3589
INHBA	Inhibin, beta A (activin A, activin AB alpha polypeptide)	3624
ISL2	ISL2 transcription factor, LIM/homeodomain, (islet-2)	64843
LDB2	LIM domain binding 2	9079
LUM	Lumican	4060
NEUROD4	Neurogenic differentiation 4	58158
SNAI1	Snail homolog 1 (*Drosophila*)	6615
SNAI2	Snail homolog 2 (*Drosophila*)	6591
SPARC	Secreted protein, acidic, cysteine-rich (osteonectin)	6678
SPRR1A	Small proline-rich protein 1A	6698

Table W1. (*continued*)

Gene Symbol	Name	Gene ID
TCF4	Transcription factor 4	6925
TLE1	Transducin-like enhancer of split 1 (E(sp1) homolog, *Drosophila*)	7088
TWIST1	twist homolog 1	7291
TWIST2	twist homolog 2	117581
WNT5A	Wingless-type MMTV integration site family, member 5A	7474
WNT5B	Wingless-type MMTV integration site family, member 5B	81029
Metabolism		
ACVR1	Activin A receptor, type I	90
ADSS	Adenylosuccinate synthase	159
AK3	Adenylate kinase 3	50808
ASNS	Asparagine synthetase	440
BHLHB2	Basic helix-loop-helix domain containing, class B, 2	8553
CD63	CD63 molecule	967
FDPS	Farnesyl diphosphate synthase	2224
FKBP14	FK506 binding protein 14, 22 kDa	55033
FMO1	Flavin containing monooxygenase 1	2326
GALK1	Galactokinase 1	2584
HSPG2	Heparan sulfate proteoglycan 2 (perlecan)	3339
INSL6	Insulin-like 6	11172
MTHFD2	Methylenetetrahydrofolate dehydrogenase ($NADP^+$ dependent) 2	10797
NME2	Nonmetastatic cells 2, protein	4831
PCK1	Phosphoenolpyruvate carboxykinase 1 (soluble)	5105
PTGIS	Prostaglandin I2 (prostacyclin) synthase	5740
PTGS1	Prostaglandin-endoperoxide synthase 1 (prostaglandin G/H synthase and cyclooxygenase)	5742
PTGS2	Prostaglandin-endoperoxide synthase 2 (prostaglandin G/H synthase and cyclooxygenase)	5743
RPS24	Ribosomal protein S24	6229
SLC3A2	Solute carrier family 3 (activators of dibasic and neutral amino acid transport), member 2	6520
SRM	Spermidine synthase	6723
VLDLR	Very low density lipoprotein receptor	7436
ZNF275	Zinc finger protein 275	10838
Biological process unknown		
ISG15	ISG15 ubiquitin-like modifier	9636
PSTPIP2	Proline-serine-threonine phosphatase interacting protein 2	9050
UPP1	Uridine phosphorylase 1	7378